A comprehensive experimental and improved kinetic modeling study on the pyrolysis and oxidation of propyne

Available online at www.sciencedirect.com

ScienceDirect

Proceedings of the Combustion Institute 38 (2021) 479–488

Proceedings of the Combustion Institute

www.elsevier.com/locate/proci

A comprehensive experimental and improved kinetic modeling study on the pyrolysis and oxidation of propyne

Snehasish Panigrahy [a,*], Jinhu Liang [a,c,*], Shashank S. Nagaraja [a], Zhaohong Zuo [d], Gihun Kim [b], Shijun Dong [a], Goutham Kukkadapu [e], William J. Pitz [e], Subith S. Vasu [b], Henry J. Curran [a]

[a] *Combustion Chemistry Centre, School of Chemistry, Ryan Institute, MaREI, National University of Ireland, Galway, Ireland*

[b] *Center for Advanced Turbomachinery and Energy Research (CATER), Mechanical and Aerospace Engineering, University of Central Florida, Orlando, FL 32816, USA*

[c] *School of Environmental and Safety Engineering, North University of China, Taiyuan, 030051, China*

[d] *College of Chemistry and Chemical Engineering, Chongqing University, 401331 Chongqing, China*

[e] *Lawrence Livermore National Laboratory, Livermore, CA 94551, USA*

Received 8 November 2019; accepted 28 June 2020
Available online 15 September 2020

Abstract

To improve our understanding of the combustion characteristics of propyne, new experimental data for ignition delay times (IDTs), pyrolysis speciation profiles and flame speed measurements are presented in this study. IDTs for propyne ignition were obtained at equivalence ratios of 0.5, 1.0, and 2.0 in 'air' at pressures of 10 and 30 bar, over a wide range of temperatures (690–1460 K) using a rapid compression machine and a high-pressure shock tube. Moreover, experiments were performed in a single-pulse shock tube to study propyne pyrolysis at 2 bar pressure and in the temperature range 1000–1600 K. In addition, laminar flame speeds of propyne were studied at an unburned gas temperature of 373 K and at 1 and 2 bar for a range of equivalence ratios. A detailed chemical kinetic model is provided to describe the pyrolytic and combustion characteristics of propyne across this wide-ranging set of experimental data. This new mechanism shows significant improvements in the predictions for the IDTs, fuel pyrolysis and flame speeds for propyne compared to AramcoMech3.0. The improvement in fuel reactivity predictions in the new mechanism is due to the inclusion of the propyne + $H\dot{O}_2$ reaction system along with $\dot{O}H$ radical addition to the triple bonds of propyne and subsequent reactions.

Keywords: Propyne oxidation; Ignition delay time; Pyrolysis; Laminar flame speed; Kinetic modeling

* Corresponding author at: Combustion Chemistry Centre, School of Chemistry, Ryan Institute, MaREI, National University of Ireland, Galway, Ireland.

E-mail addresses: snehasish.panigrahy@nuigalway.ie (S. Panigrahy), jhliang@nuc.edu.cn (J. Liang).

https://doi.org/10.1016/j.proci.2020.06.320

1. Introduction

Propyne is one of the major intermediate species in the oxidation of heavier hydrocarbon fuels and can oxidize to propargyl radicals which can recombine to benzene leading to larger poly-aromatic hydrocarbons and soot. In this context, an accurate model describing propyne kinetics over a wide range of temperatures and pressures is important to understand the formation of harmful pollutants and help produce cleaner, more efficient combustors. As novel combustion devices tend to operate in the low to intermediate temperature region, kinetic analyses through experimental and modeling studies at these conditions is vital in understanding the consumption of propyne at these conditions.

Several investigations of the oxidation of propyne have been performed using shock tubes (STs) [1,2], flow reactors [3], jet-stirred reactors (JSRs) [4,5] and a laminar flame burner [3]. Most of these studies were entirely focused on high temperature conditions. Ignition delay times (IDTs) of propyne oxidation was first measured by Radhakrishnan and Burcat [2] in a reflected ST in the temperature range 1125–2000 K at pressures ranging from 4 to 13 atm. Subsequently, Dagaut et al. [5] used a high pressure JSR to study propyne oxidation in the temperature range 900–1200 K. Davis et al. [3] measured species profiles in a turbulent flow reactor at 1170 K at equivalence ratios (φ) from 0.7 to 1.7. Curran et al. [1] performed an ignition study of propyne and allene oxidation behind reflected shock waves in the temperature range 1200–1900 K and at pressures of 2–5 bar. In addition, the oxidation of both allene and propyne were investigated in a JSR to study the identical ignition behavior and similar reactivities of the two fuels. However, Faravelli et al. [4] obtained concentration profiles of various intermediate species such as acetylene, ethylene, ethane and benzene for the oxidation of propyne and allene in a JSR and observed different oxidation behaviors of the two isomers. Only one investigation of laminar flame velocity has been reported by Davis et al. [3] for equivalence ratios ranging from 0.7 to 1.7 at atmospheric pressure and at room temperature. These studies also developed kinetic mechanisms to model their experimental measurements.

Based on the above, despite its importance, there are no IDT data available for the oxidation of propyne at low temperatures (< 900 K) and high pressures (≥ 10 bar). Moreover, there are distinct deviations between available chemical model predictions and the new IDT data measured in this work, Fig. 1. All models over-predict the IDTs by an order of magnitude, particularly in the intermediate and low temperature regime where no data existed previously. Thus, a more extensive experimental study over a wide range of operating conditions is warranted. In the present study, new IDT data for propyne auto-ignition are obtained using a rapid compression machine (RCM) and a high-pressure shock tube (HPST) ($T = 690$–1460 K, $p = 10$ and 30 bar, $\varphi = 0.5$–1.5 in air). In addition, a single-pulse shock tube (SPST) is used to study propyne pyrolysis in the temperature range of 1000–1600 K, at 2 bar. Laminar flame speeds are also determined at elevated temperature conditions for equivalence ratios in the range of 0.7–1.5. A detailed kinetic mechanism is developed and validated using the new experimental data and can predict it well. Finally, reaction pathway and sensitivity analyses are

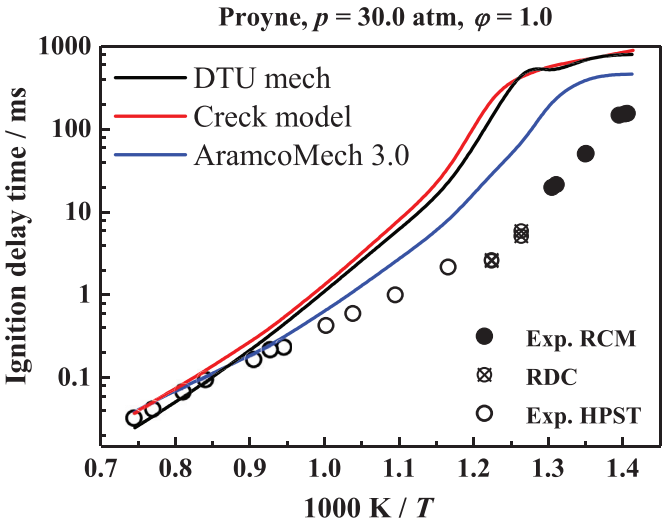

Fig. 1. Performance of various mechanisms (AramcoMech3.0 [6], DTU mech [7] and CRECK model [8]) against the IDT measured in this work (RDC: Reaction during compression period).

performed using the new model to determine the important reactions controlling propyne pyrolysis and oxidation. It is observed that reactions of propyne with hydroxyl and hydroperoxyl radicals, and subsequent chain-branching reactions of the resultant radicals are found to play a dominant role in the current kinetic mechanism.

2. Experimental work

IDT measurements for propyne oxidation were performed in a HPST and in a heated twin-opposed piston RCM at NUIG. Experiments on propyne pyrolysis were also performed using a newly developed single-pulse shock tube at NUI Galway. The flame speed experiments were carried out in a spherical vessel setup at UCF for unburned propyne/air gas temperature of $T_u = 373$ K at two different pressure conditions (1 and 2 bar). Table S-1 provides the detailed oxidation experimental conditions investigated in this work. The pyrolysis of 2% propyne was performed at 2 bar pressure in a SPST. Propyne was obtained from Sigma Aldrich with greater than 99.0% purity. Oxygen, nitrogen and argon were acquired from BOC Ireland at high purity ($\geq$ 99.5%). Krypton (99.99%) was obtained from Sigma Aldrich and was used as an internal standard gas during the pyrolysis experiments. No further purification was carried out in this study.

2.1. Pyrolysis species measurements; NUI Galway single-pulse shock tube (SPST)

The new SPST experimental setup used for this study has a 5.8 m driven section with an inner diameter of 10.24 cm. The shock heated analyte is examined using an Agilent 6890/5975 gas chromatography-mass spectrometry (GC–MS) system. The sample from the end-wall is inserted into a GS-Gaspro column through a split/split-less inlet. Helium is used as the carrier gas with a constant flow rate of 0.9 ml min^{-1}. The pyrolysis of 2% propyne was performed at 2 bar pressure in the temperature range of 1000–1800 K. Mixtures containing 2% propyne were prepared based on partial pressures in a 40 L mixing vessel. The final mixture contains 2% fuel, 0.5% Kr (internal standard) and 97.5% Ar. Ar was used as the diluent instead of N_2 to prevent the reaction of N_2 with hydrocarbon radicals and also to reduce the influence of relaxation behind the shock wave during the pyrolysis experiments. The reflected pressure and temperature conditions were obtained using GasEq [9], by providing the necessary inputs of initial pressure, temperature, composition, and shock velocity. The calculated pressures were verified using the end-wall Kistler (603CAB) pressure sensor. Using the standard GC method, the major detectable species that were quantified result in a carbon balance of > 90%. The new mechanism was used to identify the formation pathways of the quantified species via reaction flux analyses. However, no C_5 species were either detected in the experiments or predicted by the model based on the flux analyses. We were unable to detect species > C_6, because the detection limit of the GC was not low enough to detect the formation of these higher hydrocarbons in very small amounts. The uncertainties in reflected temperatures are calculated based on those in the shock velocities and are approximately ±2%. The uncertainty in calibrated species concentrations is approximately ±10% and estimated species concentrations is approximately ±20%. The uncertainty in reactant mole fractions is ±0.02%.

2.2. NUI Galway high pressure shock tube (HPST)

IDTs of propyne/'air' mixtures were measured in a HPST at equivalence ratios of 0.5, 1.0 and 2.0, at pressures of 10 and 30 bar and at intermediate to high temperatures, 900–1460 K. A detailed description of the facility was published previously [10,11] and is described briefly as Supplementary material. The IDT is defined as the interval between the rise in pressure due to the arrival of the incident shock wave at the end wall and the maximum rate of rise of the pressure signal. The largest uncertainty of temperature behind the reflected shock wave was estimated to be ±20 K, which can lead to a 20% uncertainty in measured IDTs.

2.3. NUI Galway rapid compression machine (RCM)

A heated twin-opposed piston RCM was used to the measure IDTs of propyne/'air' mixtures at equivalence ratios of 0.5, 1.0 and 2.0, at the pressures of 10 and 30 bar and in the low- to intermediate-temperature range 675–880 K. The 'air' used here is a mixture of O_2 and N_2/Ar in the molar ratio of 21/79. Details of the RCM have been provided previously [12,13]. The Supplementary material provides a brief description of the RCM setup and experimental procedure.

2.4. Laminar flame speed; UCF – spherical flame speed setup

Laminar flame speeds were measured using a spherical experimental flame speed setup that is mainly composed of a mixing tank, spherical combustion chamber, optical components, ignition circuit, and data acquisition system (details in [14–16]). Details of the experimental and mixture preparation technique are provided in the Supplementary material. In this study, laminar burning velocity was calculated by using constant volume method with multi-zone thermodynamic model. The detailed model was presented earlier papers [15,16], and brief explanation is provided here.

The multi-zone model consists of two regions: the burned and unburned mixtures. For the properties of each burned zone while combustion, equilibrium calculations are required [17]. To calculate the burned gases properties, Cantera software [18] with AramcoMech3.0 mechanism were used. After solving the properties of the burned gases, laminar burning velocity LBV are calculated from the measured pressure time-histories. Stretch effects are not considered in this study because several studies [19,20] have shown that the stretch effect is negligible using the constant volume method. The average uncertainty in measured laminar speeds were founded to be around 5.9%.

3. Kinetic modeling

The detailed chemical kinetic reaction mechanism used in these calculations is based on a newly updated model containing the H_2/O_2 sub-mechanism, along with the C_1–C_3 sub-mechanisms. The foundation of this hierarchical model is based on several prior mechanisms developed at NUIG. The kinetic model has been re-evaluated by incorporating recent advancements in rate constants and thermochemical properties by critical assessment of recently published experimental and theoretical studies. Most of the updates to the propyne sub-mechanism were carried out as part of the ongoing development of the C_1–C_3 base mechanism at NUIG. The present model includes detailed low- and high-temperature reaction mechanisms explicit to propyne chemistry. Modifications of important reactions were made and are provided as Supplementary material in NUIGMech1.0.

4. Results and discussion

Comparisons of model predictions compared to speciation data from propyne (C_3H_4-p) pyrolysis, IDT measurements, as well as laminar burning velocities at elevated temperature conditions are presented. Good agreement between the new updated model and the experimental measurements from the present work is observed. Briefly the important reactions for propyne pyrolysis, ignition and oxidation determined through sensitivity and flux analyses are discussed in detail.

Figure 2 shows the major and minor products formed in the pyrolysis of 2% propyne in a SPST at 2 bar pressure in the temperature range 1000–1800 K. Figure 2(a) presents the major products detected including methane (CH_4), allene (C_3H_4-a), and acetylene (C_2H_2). Other minor products include ethylene (C_2H_4), 1,3-butadiene (C_4H_6), vinyl acetylene (C_4H_4), diacetylene (C_4H_2) and benzene (C_6H_6), Fig. 2(b). The experimentally measured species are well predicted by the current model, whereas AramcoMech3.0 is less accurate.

Figure 3 illustrates the main reaction pathways of propyne pyrolysis at 1432 K. C_3H_4-p is primarily consumed via its chemically activated reaction with the $\dot{H}$ atoms to form C_2H_2 and $\dot{C}H_3$ radicals ($C_3H_4\text{-p} + \dot{H} \leftrightarrow C_2H_2 + \dot{C}H_3$). It also undergoes H-atom abstraction reactions by $\dot{H}$ atoms and $\dot{C}H_3$ radicals producing propargyl ($\dot{C}_3H_3$) radicals and H_2 and CH_4, via $C_3H_4\text{-p} + \dot{H} \leftrightarrow \dot{C}_3H_3 + H_2$ and $C_3H_4\text{-p} + \dot{H} \leftrightarrow \dot{C}_3H_3 + CH_4$, respectively. The CH_4 produced here is largely unreactive and accumulates during pyrolysis. Some $\dot{C}_3H_3$ radicals are also formed from $C_3H_4\text{-p} \leftrightarrow \dot{C}_3H_3 + \dot{H}$. These propargyl radicals recombine to generate benzene (C_6H_6) and fulvene, which can reproduce benzene, through fulvene $\rightleftharpoons C_6H_6$ and fulvene $+ \dot{H} \leftrightarrow C_6H_6 + \dot{H}$ reactions. The rate coefficients for all of these reactions are adopted from Miller et al. [21,22]. However, the rate constant for $C_3H_4\text{-p} + \dot{H} \leftrightarrow C_2H_2 + \dot{C}H_3$ used here is a factor of 1.5 higher than that determined by Miller et al. [22], as this improved the model agreement with the measured C_3H_4-p and C_2H_2 speciation profiles. The resultant $\dot{C}H_3$ radicals generate ethyl radicals ($\dot{C}_2H_5$), via the chemically activated pathway $\dot{C}H_3 + \dot{C}H_3 \leftrightarrow C_2H_5 + \dot{H}$, which in turn, undergoes unimolecular decomposition producing $C_2H_4 + \dot{H}$. C_2H_4 is also generated from $C_4H_6 + \dot{H} \leftrightarrow \dot{C}_2H_3 + C_2H_4$. The rate constant of this reaction is adopted from Li et al. [31] and is a factor of two lower than the rate constant used in AramcoMech3.0. This modification improved the model agreement with the C_4H_6, C_4H_4 and C_4H_2 species profiles, but leads to an under-prediction in the C_2H_4 mole fractions. C_3H_4-a is generated from the isomerization of C_3H_4-p and by the $\dot{H}$ atom catalyzed reaction $C_3H_4\text{-p} + \dot{H} \leftrightarrow C_3H_4\text{-a} + \dot{H}$. The reaction flux analysis (RFA) shows that, C_4H_6, C_4H_4 and C_4H_2 are formed from C_3H_4-p and C_3H_4-a, via the sequence 1,2-$C_4H_6 \rightarrow C_4H_6 \rightarrow \dot{C}_4H_5\text{-i} \rightarrow C_4H_4 \rightarrow \dot{C}_4H_3\text{-i} \rightarrow C_4H_2$.

Figure 4 presents the IDT measurements from the HPST and RCM for propyne in 'air' mixtures comparing the effect of equivalence ratio at pressures of 10 atm and 30 bar. The solid symbols represent the data taken in the RCM and the open symbols the data recorded in the HPST. The sold lines and dashed lines represent model predictions using NUIGMech1.0 and AramcoMech3.0, respectively. NUIGMech1.0 shows a significantly improved performance, particularly at low temperatures (< 1000 K).

Figure 4 shows that IDTs decrease with increasing temperature and equivalence ratio, as expected. However, the effect of equivalence ratio on the IDT declines with temperature. The current model captures all of the experimental

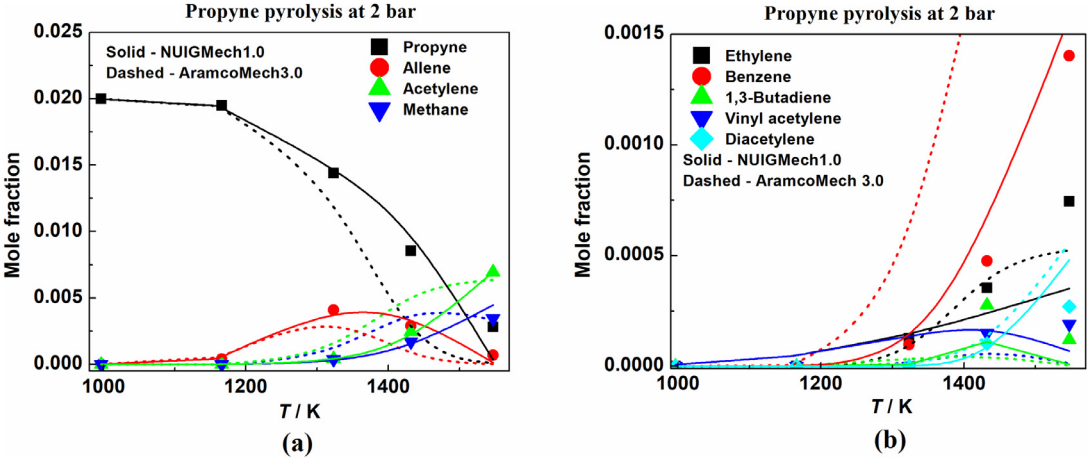

Fig. 2. Species profiles for propyne pyrolysis.

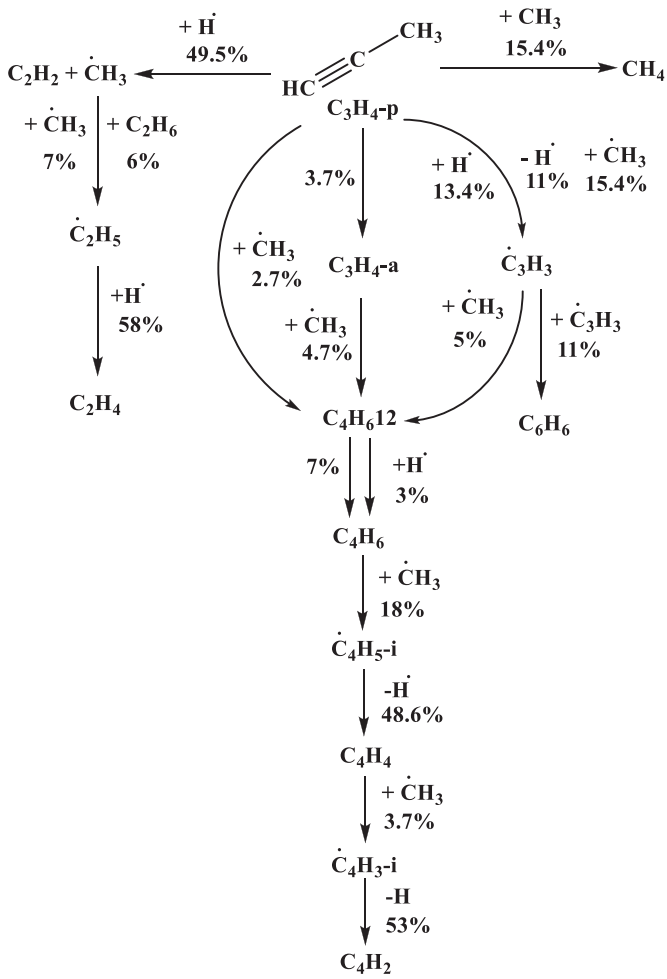

Fig. 3. Reaction flux diagram for propyne pyrolysis at 1432 K.

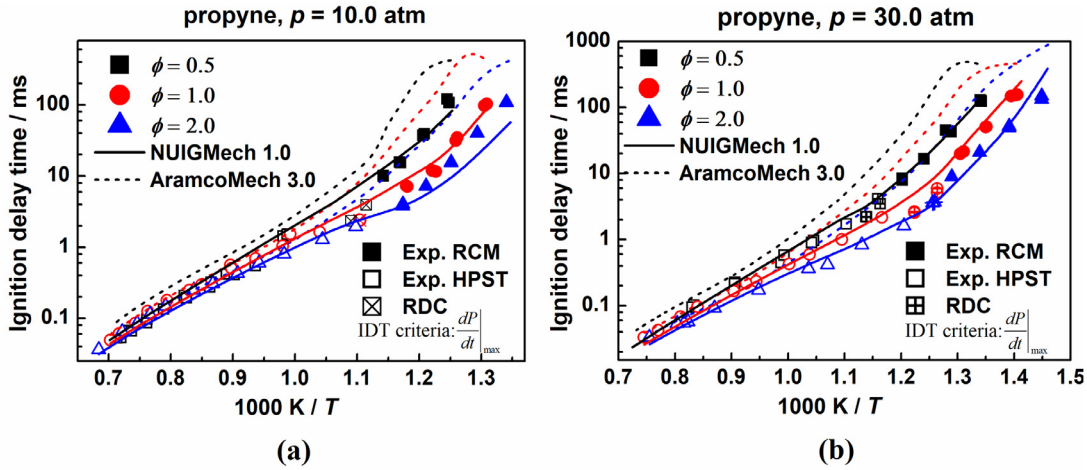

Fig. 4. IDT measurements for propyne in 'air' mixtures at (a) $p = 10$ atm and (b) $p = 30$ atm.

data trends very well but tends to under-predict reactivity at $\varphi = 2.0$ and 10 bar for the lower-temperature RCM experiments. However, generally the present model offers a better agreement compared to AramcoMech3.0.

Figure 5 illustrates flux analyses performed for C_3H_4-p ignition at different temperatures (700 K, 950 K, and 1350 K) for the results shown in Fig. 4(b) at $\varphi = 1.0$ at 30 bar. In the figure, the black symbols represents the flux at 700 K, the red symbols the flux at 950 K, and the blue symbols the flux at 1350 K. The percentage values shown in the flux diagram signifies the relative flux through the system based on 100% of the x% of propyne consumed at the condition presented. In addition, a sensitivity analysis is carried out to highlight the important reactions at this condition (Fig. S-1). The reaction pathways presented in the dashed box are responsible for the improvement in the predictions using NUIGMech1.0 and are not present in AramcoMech3.0. The flux analyses show that, at 700 K the fuel consumption process is initiated by H-atom abstraction reaction mainly by $\dot{O}H$ and $H\dot{O}_2$ radicals forming propargyl radicals. In addition to H-atom abstraction, $\dot{O}H$ addition to propyne's triple bond is the most important reaction controlling propyne reactivity at low temperatures. Rate coefficients for the $\dot{O}H$ addition reactions have been adopted from the high-level theoretical study of Zádor et al. [23]. $\dot{O}H$ radicals can add to the central or terminal carbon atom. At low temperatures the rate of $\dot{O}H$ addition to the terminal carbon atom (pC_3H_4OH-2) is four times higher than that of central carbon atom ($CH_3C(OH)CH$). The resultant $p\dot{C}_3H_4OH$-2 radical can react with O_2 to form CH_3COCHO, which eventually produces CO, $\dot{C}H_3$ and $\dot{O}H$ radicals. No experimental measurements or theoretical calculations are reported in the literature for this reaction sequence. In the present model their rate constants are estimated by the analogous $\dot{C}_2H_2OH$ radical addition to O_2 from the experimental study of Siese et al. [24].

Beside $\dot{O}H$ addition, $\dot{H}$ atoms can also add to propyne producing 1-methyl-vinyl radicals ($\dot{C}_3H_5$-t), which also plays a major role at low temperature as suggested by Miller et al. [22]. The resultant $\dot{C}_3H_5$-t radicals can add to O_2 generating C_3H_5-$t\dot{O}_2$ radicals, which subsequently produce acetyl radicals and formaldehyde or decomposes to formaldehyde, CO and methyl radicals. The rate constant of $\dot{C}_3H_5$-$t + O_2$ and the subsequent reactions are adopted from the recent work of Goldsmith et al. [25], who conducted a high-level ab-initio study at the CCSD(T)-F12a/cc-pVTZ-F12// B2PLYPD3/cc-pVTZ level of theory. In the previous model rate constant for $\dot{C}_3H_5$-$t + O_2 \leftrightarrow CH_2O + CH_3\dot{C}O$ was adopted from the estimated work of Laskin et al. [26] and was order of magnitude higher than the rate used in this study.

At higher temperatures (900 K and 1350 K) H-atom abstraction by $\dot{O}H$ and $H\dot{O}_2$ radicals becomes more important yielding propargyl radicals. These are consumed in the reaction $\dot{C}_3H_3 + O_2 \leftrightarrow CH_2CO + H\dot{C}O$, with its rate constant taken from the theoretical work of Hahn et al. [27]. Their calculated rate constant agrees well with the experimental studies of Slagle and Gutman [28] and Atkinson and Hudgens [29]. At high temperature the chemically activated pathway C_3H_4-$p + \dot{H} \leftrightarrow C_2H_2 + \dot{C}H_3$ becomes important and also contributes to the consumption of propyne. The self-isomerization and $\dot{H}$ atom catalyzed isomerization of propyne to allene, only contributes 10% to total fuel consumption at the condition studied here.

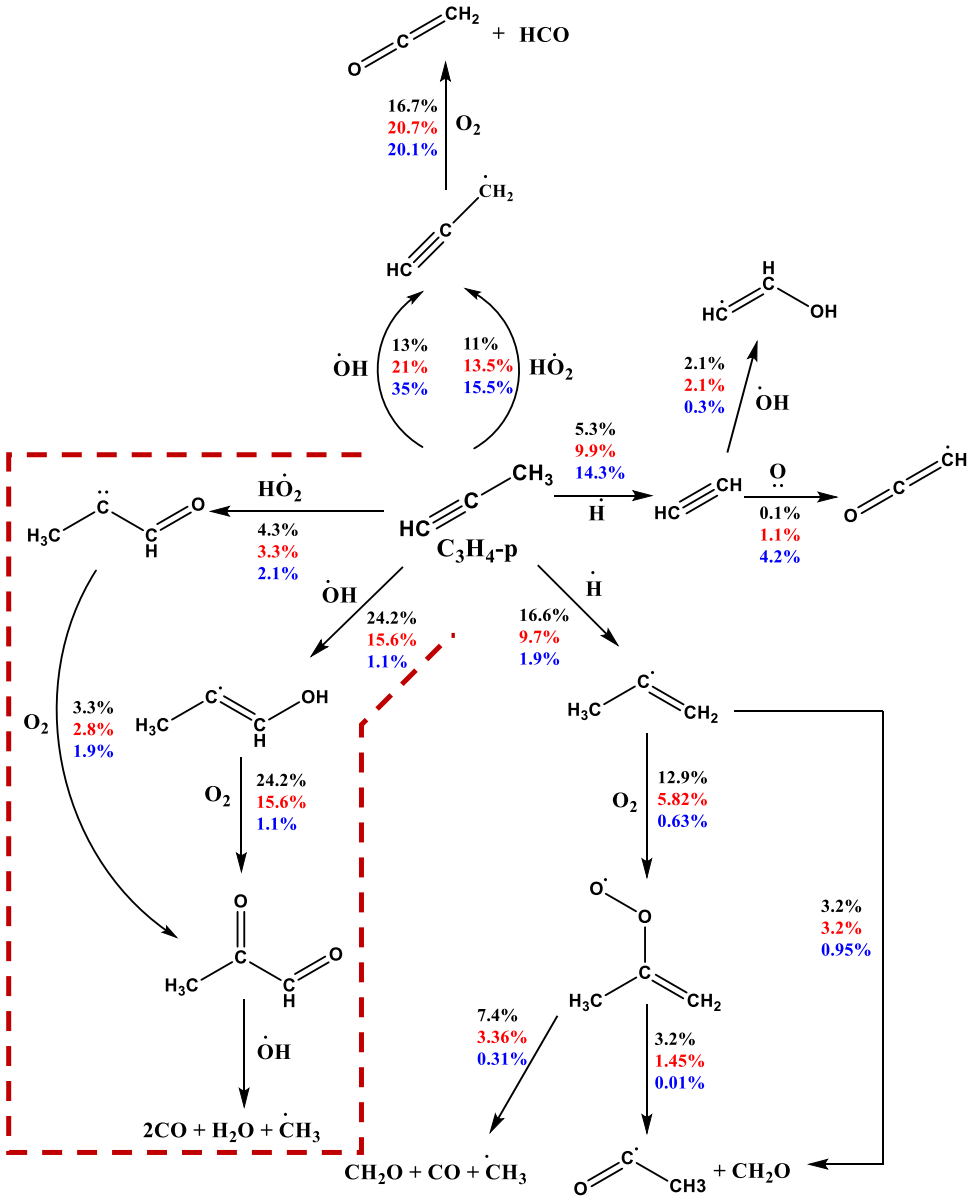

Fig. 5. Flux analyses for propyne ignition at different temperatures for $\varphi = 1.0$ at 30 bar pressure. New reaction channels included in the present model are presented with in the dashed box.

Ultimately, it is the reaction of propyne with hydroperoxyl radical which has the highest influence on model predictions. Sensitivity analysis confirms that $C_3H_4\text{-p} + H\dot{O}_2 = CH_3\dot{C}CHO + \dot{O}H$ is the most sensitive reaction that promotes reactivity (Fig. S-1). The $C_3H_4\text{-p} + H\dot{O}_2$ reactions were not included in AramcoMech3.0. Figure 6(a) clearly shows that the deviations observed when the $C_3H_4\text{-p} + H\dot{O}_2$ and succeeding reactions are included in the mechanism. This suggests that the improvement in the predictions using NUIGMech1.0 is mainly attributable to the inclusion of the chain branching reaction $C_3H_4\text{-p} + H\dot{O}_2 = CH_3\dot{C}CHO + \dot{O}H$. The resultant $CH_3\dot{C}CHO$ radicals react with molecular oxygen producing 2-oxo propanal (CH_3COCHO) and Ö atoms that increases the reactivity of the system. Rate coefficients for these pressure and temperature dependent reactions are taken by analogy with acetylene with $H\dot{O}_2$ radical from the theoretical investigation of Gimenez-Lopez et al.

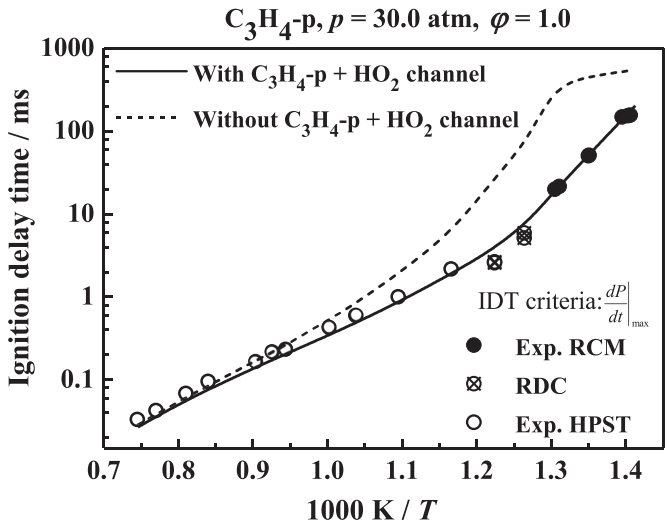

Fig. 6. (a) Effect of C_3H_4-p + $H\dot{O}_2$ reaction on IDT prediction.

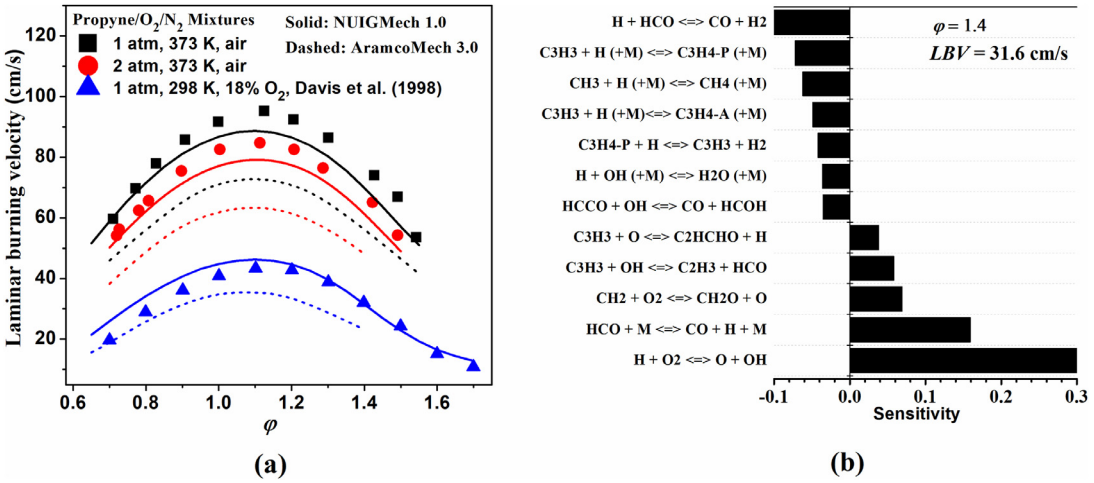

Fig. 7. (a) Laminar flame speed of propyne/'air' at 1 and 2 atm for $T_u = 298$ K and 373 K. (b) Flame speed sensitivity analysis at $\varphi = 1.4$.

[30]. 2-oxo propanal subsequently decomposes to form CO, H_2O and $\dot{C}H_3$. $\dot{C}H_3$ subsequently produces CO via, $CH_3\dot{O} \rightarrow CH_2O \rightarrow H\dot{C}O \rightarrow CO$, and finally CO reacts with $\dot{O}H$ producing CO_2 through $CO + \dot{O}H = CO_2 + \dot{H}$, which is a highly exothermic reaction that further enhances reactivity.

Figure 7 shows the measured and predicted laminar burning velocities for propyne in air at 1 and 2 bar and at $T_u = 373$ K. Moreover, experimental [3] and calculated laminar flame speeds for propyne/N_2/O_2 mixtures (18% O_2 in N_2) at atmospheric pressure and at room temperature ($T_u = 298$ K) are reported for comparison in Fig. 7. The laminar flame speed studied by Davis et al. [3] was measured using a counterflow twin flame technique. Reference [3] addresses the details of the technique employed to study the laminar flame speeds for propyne/N_2/O_2 mixtures. In comparison to NUIGMech1.0, AramcoMech3.0 severely under-predicts the flame speed for all experimental data across the range of equivalence ratios. The present mechanism can accurately predict the UCF flame speed data for the fuel-lean experiments; however, it under-predicts the flame speed for the fuel-rich data. Whereas, the opposite trend can be observed for the current model prediction against those measured for the 18% O_2 case. Sensitivity analyses of reaction rate constants to flame speeds shows many of the important re-

actions highlighted in the analysis belong to the H_2/CO sub-mechanism such as reactions between $\dot{H}$ atoms and O_2, formyl radical reacting with $\dot{H}$ atoms, etc. The sensitive fuel specific reactions include $\dot{C}_3H_3 + \dot{H}$ (+M) ↔ C_3H_4-p (+M) and C_3H_4-p + $\dot{H}$ ↔ $\dot{C}_3H_3 + H_2$ (Fig. 7(b)). These reactions inhibit reactivity because they consume $\dot{H}$ atoms in competition with the main chain branching reaction $H^{\cdot} + O_2 \leftrightarrow \ddot{O} + O\dot{H}$. It should be noted that the rate constant for $\dot{C}_3H_3 + \dot{H}$ (+M) ↔ C_3H_4-p (+M) used here is reduced by a factor of two compared to that calculated by Miller et al. [21] to gain agreement with the flame speed data on the fuel-rich side. This modification also improved propyne pyrolysis predictions as discussed above.

5. Conclusions

In this paper, new experimental measurements for propyne auto-ignition are reported using a rapid compression machine and a high-pressure shock tube for temperatures in the range 750–1300 K at compression pressures of 10 and 30 bar and equivalence ratios in the range 0.5–2.0. A single-pulse shock tube was utilized to study propyne pyrolysis in the temperature range 1000–1600 K, at 2 bar pressure. Additionally, laminar burning speeds were also measured at elevated temperature conditions for equivalence ratios in the range 0.7–1.5. A new chemical kinetic model, NUIGMech1.0, has been validated against the experimental studies conducted in the present work (RCM; shock-tube IDTs; flame speeds and pyrolysis speciation). Important reactions are highlighted through sensitivity and flux analyses. C_3H_4-p + $H\dot{O}_2$ and C_3H_4-p + $\dot{O}H$ addition reactions are found to be important for propyne oxidation, particularly at low- to intermediate temperature and high-pressure (≥ 10 bar) conditions. Rate coefficients have been implemented from the most recent inclusive experimental and theoretical studies. Nevertheless, some rate constants are estimated based on analogy for the reactions where no data is available in the literature.

Declaration of Competing Interest

None.

Acknowledgments

The authors would like to acknowledge Science Foundation Ireland for funding via project numbers 15/IA/3177 and 16/SP/3829. The material for measuring flame speed is based upon work supported by the U.S. Department of Energy's Office of Energy Efficiency and Renewable Energy (EERE) under Award Number DE-EE0007984 (Co-Optima). Jinhu Liang acknowledges the International Scientific Cooperation Projects of Key R&D Programs in Shanxi Province via project number 201803D421101 and Research Project Supported by Shanxi Scholaiship Council of Chinavia project number 2020-115. We want to acknowledge Tyler MacDougall of University of Central Florida for his help with LBV experiments.

Disclaimer

Supplementary materials

Supplementary material associated with this article can be found, in the online version, at doi:10.1016/j.proci.2020.06.320.

References

[1] H.J. Curran, J.M. Simmie, P. Dagaut, D. Voisin, M. Cathonnet, *Proc. Combust. Inst.* 26 (1996) 613–620.
[2] K. Radhakrishnan, A. Burcat, *Combust. Sci. Technol.* 54 (1987) 85–101.
[3] S.G. Davis, C.K. Law, H. Wang, *Symp. (Int.) Combust.* 27 (1998) 305–312.
[4] T. Faravelli, A. Goldaniga, L. Zappella, E. Ranzi, P. Dagaut, M. Cathonnet, *Proc. Combust. Inst.* 28 (2000) 2601–2608.
[5] P. Dagaut, M. Cathonnet, J.-.C. Boettner, *Combust. Sci. Technol.* 71 (1990) 111–128.
[6] C.-.W. Zhou, Y. Li, U. Burke, C. Banyon, K.P. Somers, S. Khan, J.W. Hargis, T. Sikes, E.L. Petersen, M. Alabbad, A. Farooq, Y. Pan, Y. Zhang, Z. Huang, J. Lopez, Z. Loparo, S.S. Vasu, H.J. Curran, *Combust. Flame* 197 (2018) 423–438.
[7] H. Hashemi, J.M. Christensen, L.B. Harding, S.J. Klippenstein, P. glarborg, *Proc. Combust. Inst.* 37 (1) (2019) 461–468.

[8] E. Ranzi, A. Frassoldati, R. Grana, A. Cuoci, T. Faravelli, A.P. Kelley, C.K. Law, *Prog. Energy Combust. Sci.* 38 (4) (2012) 468–501.
[9] C. Morley, Gaseq, Version 0. 76, (2004).
[10] H. Nakamura, D. Darcy, M. Mehl, C.J. Tobin, W.K. Metcalfe, W.J. Pitz, C.K. Westbrook, H.J. Curran, *Combust. Flame* 161 (2014) 49–64.
[11] S.M. Burke, U. Burke, R. Mcdonagh, O. Mathieu, I. Osorio, C. Keesee, A. Morones, E.L. Petersen, W.J. Wang, T.A. Deverter, M.A. Oehlschlaeger, B. Rhodes, R.K. Hanson, D.F. Davidson, B.W. Weber, C.J. Sung, J. Santner, Y.G. Ju, F.M. Haas, F.L. Dryer, E.N. Volkov, E.J.K. Nilsson, A.A. Konnov, M. Alrefae, F. Khaled, A. Farooq, P. Dirrenberger, P.A. Glaude, F. Battin-Leclerc, H.J. Curran, *Combust. Flame* 162 (2015) 296–314.
[12] L. Brett, *Re-commissioning of a rapid compression machine and computer modelling of hydrogen and methane autoignition.Ph.D. Thesis*, National University of Ireland, Galway, 1999.
[13] L. Brett, J. Macnamara, P. Musch, J.M. Simmie, *Combust. Flame* 124 (2001) 326–329.
[14] G. Kim, B. Almansour, S. Park, A.C. Terracciano, K. Zhang, S. Wagnon, W.J. Pitz, S.S. Vasu, in: Advances and Current Practices in Mobility: SAE International Conference Proceedings in press(SAE Technical Paper 2019-01-0571), 2019.
[15] B. Almansour, G. Kim, S. Vasu, *SAE Int. J. Fuels Lubric.* (2018).
[16] B. Almansour, S. Alawadhi, S. Vasu, *SAE Int. J. Fuels Lubric.* 10 (2) (2017) 432–441.
[17] K. Saeed, C. Stone, *Combust. Flame* 139 (1) (2004) 152–166.
[18] H.K.M. David G. Goodwin, and R.L. Speth., Cantera: an object- oriented software toolkit for chemical kinetics, thermodynamics, and transport processes, 2016. http://www.Cantera.Org (Accessed Version 2.2.1.)
[19] A. Moghaddas, K. Eisazadeh-Far, H. Metghalchi, *Combust. Flame* 159 (4) (2012) 1437–1443.
[20] E. Rokni, A. Moghaddas, O. Askari, H. Metghalchi, *J. Energy Res. Technol.* 137 (2015) 012–204.
[21] J.A. Miller, S.J. Klippenstein, *J. Phys. Chem. A.* 107 (2003) 2680–2692.
[22] J.A. Miller, J.P. Senosiain, S.J. Klippenstein, Y. Georgievskii, *J. Phys. Chem. A* 112 (2008) 9429–9438.
[23] J. Zador, J.A. Miller, *Proc. Combust. Inst.* 35 (2015) 181–188.
[24] M. Siese, C. Zetzsch, *Z. Phys. Chem.* 188 (1995) 75–89.
[25] X. Chen, C.F. Goldsmith, *J. Phys. Chem. A* 121 (48) (2017) 9173–9184.
[26] A. Laskin, H. Wang, C.K. Law, *Int. J. Chem. Kinet.* 32 (10) (2000) 589–614.
[27] D.K. Hahn, S.J. Klippenstein, J.A. Miller, *Faraday Discuss.* 119 (2002) 79–100.
[28] I.R. Slagle, D. Gutman, *Proc. Combust. Inst.* 21 (1986) 875.
[29] D.B. Atkinson, J.W. Hudgens, *J. Phys. Chem. A* 103 (21) (1999) 4242–4252.
[30] J.G. Lopez, C.T. Rasmussen, H. Hashemi, M.U. Alzueta, Y. Gao, P. Marshall, C.F. Goldsmith, P. Glarborg, *Int. J. Chem. Kinet.* 48 (11) (2016) 724–738.
[31] Y. Li, S.J. Klippenstein, C-W. Zhou, H.J. Curran, *J. Phys. Chem. A* (121) (2017) 7433–7445.